We are IntechOpen, the world's leading publisher of Open Access books
Built by scientists, for scientists

4,800
Open access books available

122,000
International authors and editors

135M
Downloads

Our authors are among the

154
Countries delivered to

TOP 1%
most cited scientists

12.2%
Contributors from top 500 universities

CLARIVATE ANALYTICS
BOOK CITATION INDEX
INDEXED

WEB OF SCIENCE™

Selection of our books indexed in the Book Citation Index in Web of Science™ Core Collection (BKCI)

Interested in publishing with us?
Contact book.department@intechopen.com

Numbers displayed above are based on latest data collected.
For more information visit www.intechopen.com

11

Application of Sliding Mode Control to Friction Compensation of a Mini Voice Coil Motor

Shir-Kuan Lin[1], Ti-Chung Lee[2] and Ching-Lung Tsai[1]
[1]*Department of Electrical Engineering, National Chiao Tung University*
[2]*Department of Electrical Engineering, Minghsin University*
Taiwan

1. Introduction

This chapter deals with the position control of a mini voice coil motor (VCM) mounted on a compact camera module (CCM) of a mobile phone. Mini VCMs are increasingly popular nowadays in 3C electronic gadgets such as mobile phones, digital cameras, web cams, etc. (Yu et al., 2005). The common requirements of these gadgets are miniaturization and high performance. Miniaturized VCM faces the challenge of accuracy position control. Sliding mode control will be adopted to compensate for the nonlinear friction in the actuator of the VCM. Experimental results in this chapter will show that good position control performance is achieved by sliding mode control.

Fig. 1 shows such a typical VCM with the size of 8.5×8.5×4.6 mm^3 and the stroke of 0.35mm. In Fig. 1(b), the congeries of the magnet (a), the yoke (d), and the lens holder (e) forms the actuator, while the guide pins (b), the coils (c), and the CMOS sensor cover (f) are stationary parts. The current through the coils generates force to move the actuator along the guide pins, which induces nonlinear friction. It is known that friction is the cause of stick slip oscillations during the motion when a usual PI controller is applied to the VCM.

The work (Bona & Indri, 2005) presents a comprehensive survey of different kinds of friction compensation schemes, and indicates that types A and B solutions are suitable for cost-sensitive applications because of its limited calculation burden. Several other methods in the literature are a nonlinear proportional controller with bang-bang force in specified region to compensate for the stick slip friction (Southward et al., 1991) , a look-up table position controller with higher gain for smaller position error and lower gain for larger position error to eliminate stick slip oscillations (Hsu et al., 2007), and an anti-windup PI controller, incorporated with the disturbance observer, to control a VCM (Lin et al., 2008).

To overcome the load variation due to tilt attitude of the CCM and the nonlinear friction force of the VCM, a dedicated sliding mode controller will be designed for the position control. High accuracy repeatability under 10 μm, fast settling time, and free of stick slip oscillations are the control goals. The challenge of the sliding mode controller design for the VCM is to select the control gains such that the error state variable in the sliding surface $s = 0$ will approach zero as time approaches infinite. The final value approach is used to make sure that the error state variable is bounded and can be made as small as possible by

increasing control gains. In practical implementation, if the allowable steady-state error is given, the control gains can be easily calculated out.

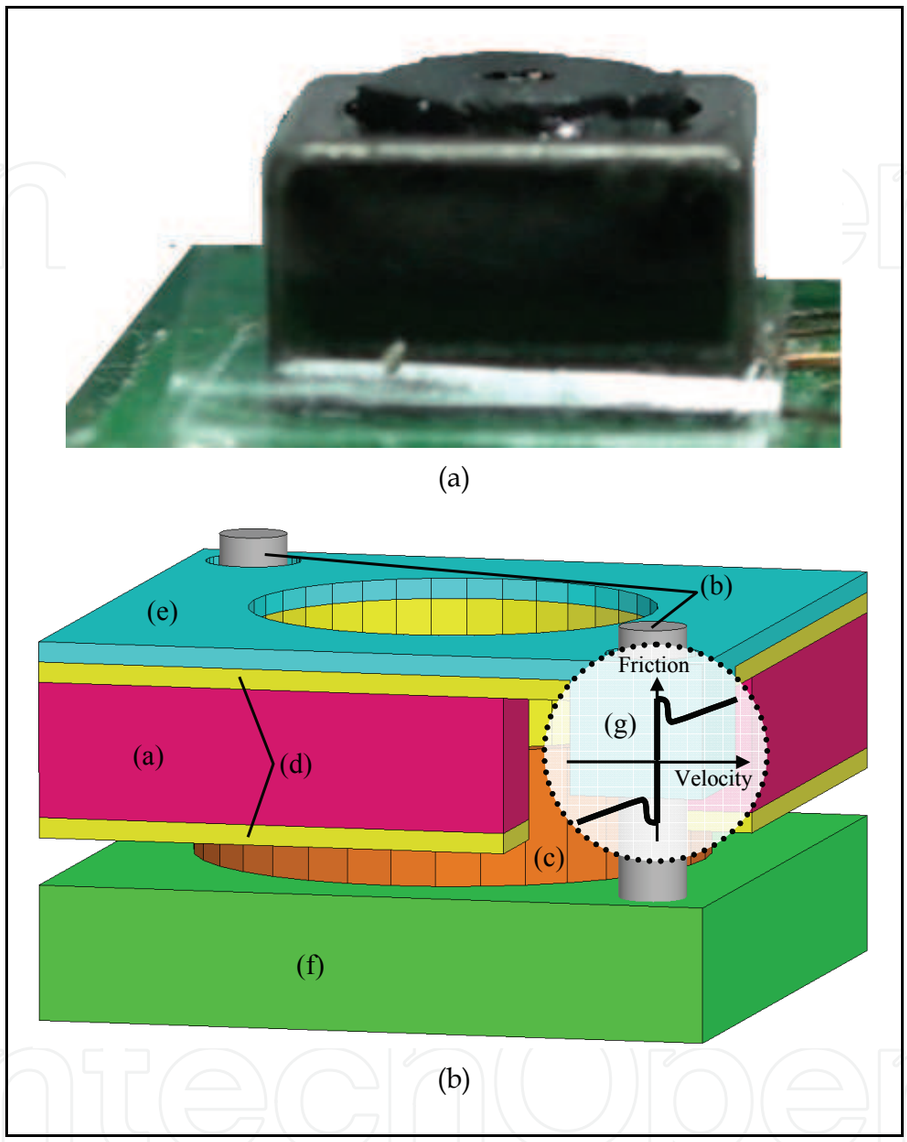

Fig. 1. Mini voice-coil motor with 8.5×8.5×4.6 mm³: (a) photo; (b) illustration of the components

2. Mathematical model of the VCM

Let the position of the actuator be d, and the current of the coils be i. The mathematical model of the VCM in Fig. 1 can be described by the dynamical and the electrical equations as follows:

$$m\ddot{d} + B\dot{d} = K_C i - f_D \tag{1}$$

$$L\dot{i} + Ri = u - K_b\dot{d} \tag{2}$$

where m and f_D are, respectively, the mass and the friction of the actuator, B is the viscous coefficient, L and R are, respectively, the inductance and the resistance of the coils, K_C is the magnetic force constant, K_b is the back-emf constant, and u is the input voltage.
Assume that the desired position is d^*. To transform Eqs. (1) and (2) into the form of state equations, we introduce the state variables of

$$x_1 = d - d^*, \quad x_2 = \dot{d}, \quad x_3 = i \tag{3}$$

and the parameters of

$$\alpha_1 = \frac{-B}{m}, \alpha_2 = \frac{K_C}{m}, \alpha_3 = \frac{-1}{m}, \alpha_4 = \frac{-K_b}{L}, \alpha_5 = \frac{-R}{L}, \alpha_6 = \frac{1}{L} \tag{4}$$

The VCM model of Eqs. (1) and (2) can then be rewritten in the form of

$$\begin{cases} \dot{x}_1 = x_2 \\ \dot{x}_2 = \alpha_1 x_2 + \alpha_2 x_3 + \alpha_3 F_D \\ \dot{x}_3 = \alpha_4 x_2 + \alpha_5 x_3 + \alpha_6 u \end{cases} \tag{5}$$

In the VCM system, x_1 is the output as well. The system turns out to be an output regulation problem with a mismatched condition, since F_D and u are in the different equations. The usual compensation and cancellation method cannot be used to eliminate F_D.
It is known (Canudas de Wit et al., 1995) that the friction F_D consists of the stiffness and the damping parts in the form of

$$F_D = \sigma_0 z + \sigma_1 \dot{z} \tag{6}$$

where σ_0 and σ_1 are the stiffness and the damping coefficients of Stribeck effect, and z is average deflection of the bristles. Let F_C be the coulomb friction force, F_S be the static friction force and v_S be the Stribeck velocity. Define the function $g(x_2)$ as

$$g(x_2) = \frac{1}{\sigma_0}\left(F_C + (F_S - F_C) e^{-\left(x_2 / v_S\right)2} \right) \tag{7}$$

Thus, the dynamic equation of z is

$$\dot{z} = x_2 - \frac{|x_2|}{g(x_2)} z \tag{8}$$

3. Sliding mode control law

The key technique of sliding mode control is to find a sliding surface in which any value of the state x_1 will move toward zero, i.e., zero position error. And then a control law is designed to drive any state variables outside the sliding surface to drop on the surface and to adhere to the surface. In such a way, the sliding mode position controller regulates the position of the actuator d to the desired one d^*.

It will be shown later that any x_1 in the sliding surface $S = 0$ will eventually approach zero, where

$$S = x_2 - \beta_1 x_1 - \beta_2 x_3 \tag{9}$$

with proper constants β_1 and β_2. The surface $S = 0$ is then the desired sliding surface of the VCM model (5).

The next mission is to design a switching input u in Eq. (5) that drives the state variables of the system to the sliding surface $S = 0$. We define $V(s) = S^2/2$, which is greater than 0 for $S \neq 0$. According to Lyapunov's stability theorem, if we can find a controller $u(x_1, x_2, x_3)$ such that $\dot{V}(0) = 0$ and $\dot{V}(s) = S\dot{S} < 0, \forall S \neq 0$, then $S = 0$ is an asymptotically stable equilibrium.

Taking derivative of Eq. (9) and substituting Eq. (5) into it, we obtain

$$\dot{S} = \left(\alpha_1 - \alpha_4\beta_2 - \beta_1\right)x_2 + \left(\alpha_2 - \alpha_5\beta_2\right)x_3 - \alpha_6\beta_2 u + \alpha_3 F_D \tag{10}$$

The first two terms on the right-hand side of Eq. (10) can be easily eliminated by directly inserting them in $u(x_1, x_2, x_3)$, since x_2 and x_3 are available states and can be used as feedback signals. However, the value of F_D is not available, so that to eliminate it needs a sufficiently large constant value. This motivates us to select

$$u = \frac{1}{\alpha_6\beta_2}\left[\left(\alpha_1 - \alpha_4\beta_2 - \beta_1\right)x_2 + \left(\alpha_2 - \alpha_5\beta_2\right)x_3 + c_1^+ \operatorname{sgn}(S) + c_2^+ S\right] \tag{11}$$

where sgn(S) is the sign of S, and c_1^+ and c_2^+ are nonnegative constants. Substituting Eq. (11) into Eq. (10) yields

$$\dot{S} = -c_2^+ S - c_1^+ \operatorname{sgn}(S) + \alpha_3 F_D \tag{12}$$

It is apparent that c_1^+ sgn(S) can be used to cancel the divergent part of $\alpha_3 F_D$, while c_2^+ provides a freedom to adjust the convergent speed. Finally,

$$\begin{aligned} \dot{V} = S\dot{S} &= -c_2^+ S^2 - c_1^+ S\operatorname{sgn}(S) + \alpha_3 F_D S \\ &\leq -c_1^+ |S| + |\alpha_3 F_D S| = -\left(c_1^+ - |\alpha_3 F_D|\right)\,|S| \\ &\leq -\left(c_1^+ - |\alpha_3| F_D^{\max}\right)\,|S| \end{aligned} \tag{13}$$

where $F_D^{\max}$ is the static friction and $F_D^{\max} \geq |F_D|$. Choose

$$c_1^+ > |\alpha_3| F_D^{\max} \tag{14}$$

to obtain $\dot{V} < 0$ for $S \neq 0$. Consequently, $u(x_1, x_2, x_3)$ in Eq. (11) with c_1^+ satisfying Eq. (14) is a controller for the asymptotically stability of $S = 0$. The approaching speed can be assigned by $c_2^+ > 0$. Moreover, we have the following theorem.

Theorem 1. Consider the VCM model of Eq. (5). Suppose that the upper bound of $F_D^{\max} \geq |F_D|$ is known. The controller $u(x_1, x_2, x_3)$ in Eq. (11) with S defined in Eq. (9), $c_1^+ > |\alpha_3| F_D^{\max}$, and $c_2^+ \geq 0$ makes the steady state value $x_1(\infty)$ of the system converge to a bounded region of

$$\left|x_1(\infty)\right| \le \frac{\left|\alpha_3\right| F_D^{\max}}{\lambda^2} \tag{15}$$

where $\lambda > 0$ is a constant, if β_1 and β_2 in (9) are

$$\beta_1 = \frac{-\lambda^2}{2\lambda + \alpha_1}, \quad \beta_2 = \frac{-\alpha_2}{2\lambda + \alpha_1} \tag{16}$$

Proof. We just need to prove that any states in the sliding surface S=0 will eventually converge to the region of Eq. (15).
It follows from Eq. (9) that in the sliding surface $S = 0$,

$$x_3 = \frac{x_2}{\beta_2} - \frac{\beta_1}{\beta_2} x_1 \tag{17}$$

Substituting Eq. (17) into the VCM model of Eq. (5), we reduce the state equation to a second-order differential equation:

$$\ddot{x}_1 - \left(\alpha_1 + \frac{\alpha_2}{\beta_2}\right)\dot{x}_1 + \frac{\alpha_2\beta_1}{\beta_2} x_1 = \alpha_3 F_D \tag{18}$$

We take Laplace transform of above equation to obtain

$$X_1(s) = \frac{s x_1(0) + \dot{x}_1(0) - \left(\alpha_1 + \frac{\alpha_2}{\beta_2}\right) x_1(0) + L\left[cF_D(t)\right]}{s^2 - \left(\alpha_1 + \frac{\alpha_2}{\beta_2}\right)s + \frac{\alpha_2\beta_1}{\beta_2}} \tag{19}$$

Substituting Eq. (16) into the characteristic equation of (19) yields

$$s^2 + 2\lambda s + \lambda^2 = 0 \tag{20}$$

which has double roots of $-\lambda < 0$. The time-domain solution to Eq. (19) is then (Golnaraghi & Kuo, 2009)

$$x_1(t) = k_1 e^{-\lambda t} + k_2 t e^{-\lambda t} + \int_0^\infty \alpha_3 F_D(t-\tau)\tau e^{-\lambda\tau} d\tau \tag{21}$$

where k_1 and k_2 are some constants. The final value of of x_1 as $t \to \infty$ is then

$$\begin{aligned} \left|x_1(\infty)\right| &= \lim_{t\to\infty}\left|\int_0^\infty \alpha_3 F_D(t-\tau)\tau e^{-\lambda\tau} d\tau\right| \\ &\le \left|\alpha_3\right| F_D^{\max} \int_0^\infty \tau e^{-\lambda\tau} d\tau = \left|\alpha_3\right| F_D^{\max}\left(-\frac{\tau e^{-\lambda\tau}}{\lambda} - \frac{e^{-\lambda\tau}}{\lambda^2}\right)\Bigg|_0^\infty \\ &= \frac{\left|\alpha_3\right| F_D^{\max}}{\lambda^2} \end{aligned} \tag{22}$$

This completes the proof. ■

Theoretically, the bounded region Eq. (15) of the steady state value $x_1(\infty)$ can be made as small as possible by increasing λ. In a practical problem, the bound of $F_D^{\max}$ and the value of α_3 are known *a priori*, so λ can be calculated out from Eq. (15) for a given bound of $x_1(\infty)$. However, the larger λ is, the larger is the absolute value of β_1, and then the larger is those of S in Eq. (9) and the controller u in Eq. (11). To limit the controller u, a control gain switching strategy is implemented. A threshold value $x_{\text{th}} > 0$ is defined first. As the sliding mode control starts up, a low-value λ is used until $|x_1| < x_{\text{th}}$. Thereafter a high-value λ is used to reduce the convergent bounded region. It can be expected that $|x_2|$ is small after $|x_1| < x_{\text{th}}$, since x_2 is the time derivative of x_1. This imples that the absolute values of $\beta_1 x_1$ and $\beta_1 x_2$ are small after $|x_1| < x_{\text{th}}$., and so are S and u. The overall sliding mode control law incorporated with the control gain switcihing strategy is illustrated in Fig. 2. There are two controllers in Fig. 2. One with low gains is outputted to the VCM for $|x_1| \geq x_{\text{th}}$, while the output to the VCM for $|x_1| < x_{\text{th}}$ is the other with high gains.

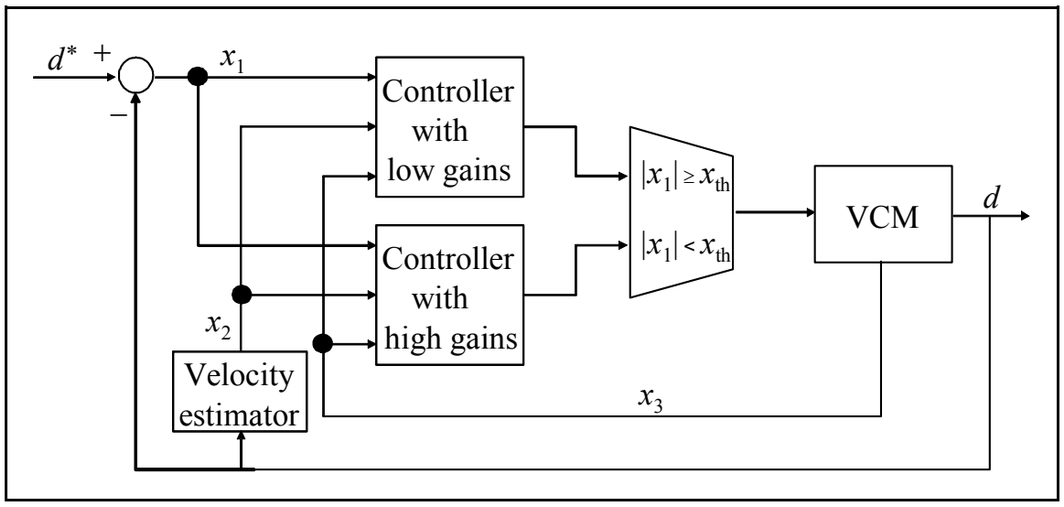

Fig. 2. Block diagram of the overall control law.

It should be remarked that the undesired chattering of the sliding mode control can be alleviated by replacing sgn(s) in Eq. (11) with the following saturation function of

$$\text{sat}(S) = \begin{cases} 1, & \text{for } S > k \\ \dfrac{S}{k}, & \text{for } |S| \leq k \\ -1, & \text{for } S < -k \end{cases} \tag{23}$$

where $k > 0$ represents the thickness of the boundary layer.

4. Simulations

Consider a real VCM which will be used in the experiments. The parameters of the VCM are $\alpha_1 = -24$, $\alpha_2 = 800$, $\alpha_3 = -1000$, $\alpha_4 = -2666.7$, $\alpha_5 = 66666.7$, $\alpha_6 = 3333.3$, $F_D^{\max} = 0.011$. Assume that the design goal is to make the steady state error smaller than 0.4 μm, which in turn asks $\lambda = 5244.044$ by Eq. (15). Substituting the value of λ into Eq. (16), we obtain $\beta_1 = -2628.036$

and β_2 = -0.076. Of course, these are high control gains. The low control gains are assigned as λ = 1172.6, β_1 = -592.36, and β_2 = -0.3446, while x_{th} = 1.5 um is chosen. We let $c_2^+ = 0$ to observe the effectiveness of c_1^+. First, choose $c_1^+ = 70 > |\alpha_3| F_D^{max} = 11$.

In the computer simulation, the VCM is modelled by Eq. (5) with the friction model of Eqs. (6)-(8). The Simulation result for the proposed controller in Theorem 1 is shown in Fig. 3. There is a steady state error $x_1(\infty) = d(\infty) - d^*$ of 0.0973 μm, which is less than the design goal of 0.4μm. This shows that the controller proposed in Theorem 1 can have the response satisfying an assigned steady state error by choosing λ from Eq. (15). On the other hand, the value of c_1^+ has the ability to drive the system states to the sliding surface $S = 0$, which can also be seen from Fig. 3, too. Actually, $S(t) = 0$ for $t > 0.009$ s. It is remarkable that the usual stick slip phenomena of the friction does not appear in the response of the proposed sliding mode controller.

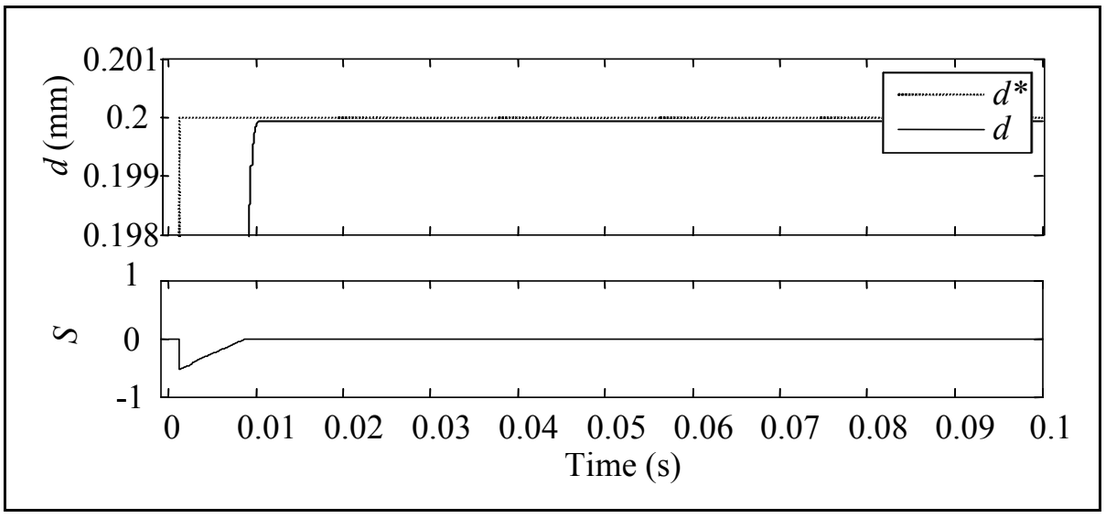

Fig. 3. Simulation response of the proposed sliding mode controller.

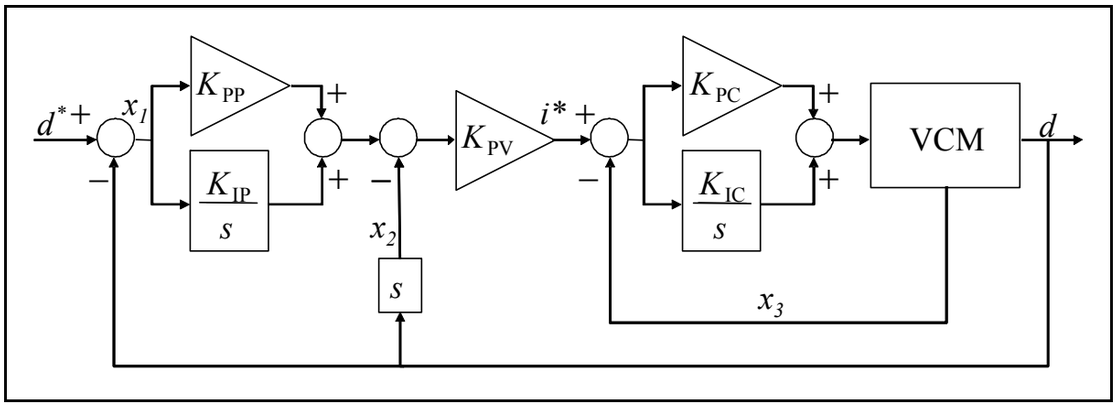

Fig. 4. Block diagram of a classic PI control law.

To show that stick slip phenomena of the friction appear in a usual controller, a classic PI control law is also simulated. The block diagram of the PI controller is shown in Fig. 4. There are two PI control loops. The inner one is the current control loop:

$$U(s) = \left(K_{\mathrm{PC}} + \frac{K_{\mathrm{IC}}}{s} \right) \left(I^*(s) - X_3(s) \right) \tag{24}$$

where $I^*(s)$ is the Laplace transform of $i^*(t)$, which is the output of the position control loop:

$$I^*(s) = K_{\mathrm{PV}} \left[\left(K_{\mathrm{PP}} + \frac{K_{\mathrm{IP}}}{s} \right) X_1(s) - X_2(s) \right] \tag{25}$$

Fig. 5(a) shows the simulation result of the classic PI controller for 0 s ≤ t ≤ 1.5 s, while its transient part before t < 0.02 s is shown in Fig. 5(b). It is apparent from Fig. 5(a) that there are stick slip oscillations in the steady-state of the classic PI controller. For the purpose of comparison, Fig. 5(c) and 5(d) show the counterparts of the simulation result of the sliding mode controller. It can be seen from Fig. 5(c) that the proposed sliding mode controller does not induce any stick slip oscillations. Besides the ability to compensate for the nonlinear friction force of the VCM, the proposed controller also has faster transient response, which can be obtained by comparing Fig. 5(d) with 5(b).

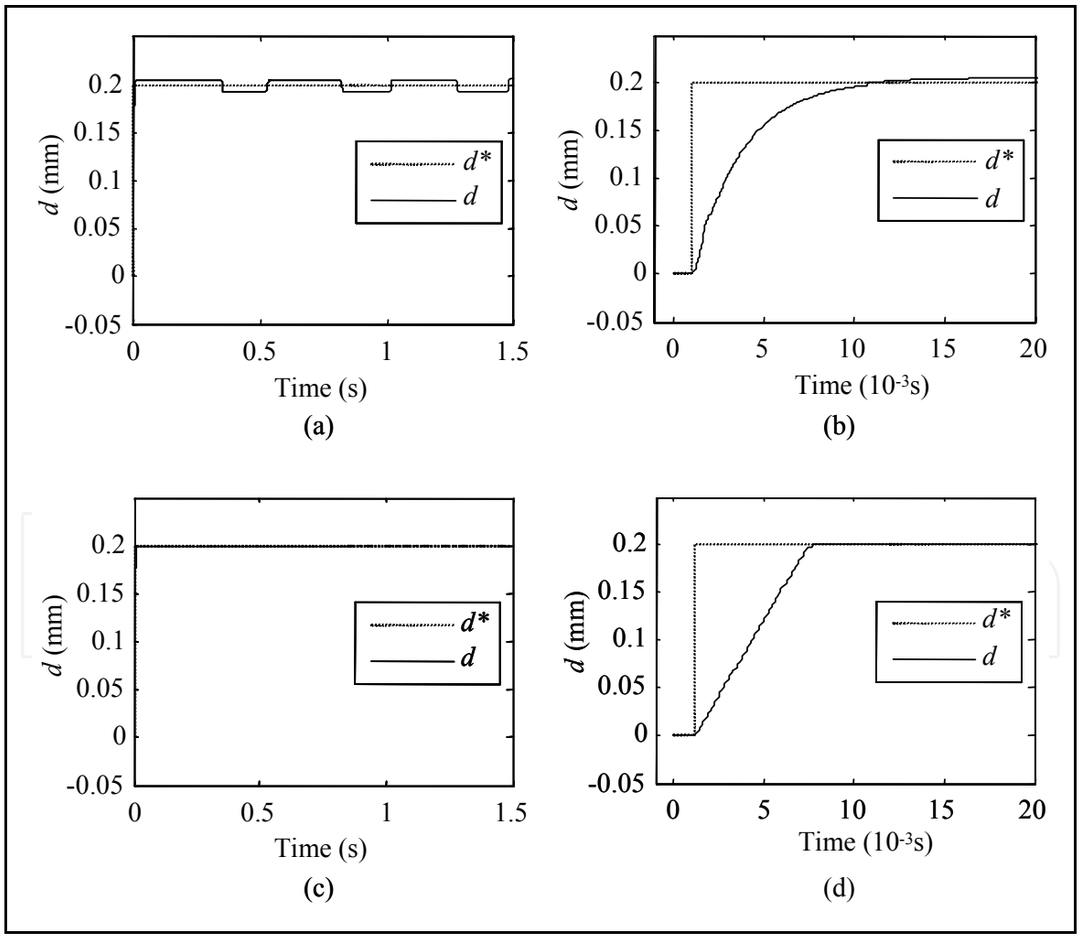

Fig. 5. Classic PI controller: (a) steady response with stick slip and (b) transient response; sliding mode controller: (c) steady response without stick slip and (d) transient response.

Furthermore, a simulation is performed to observe how c_2^+ in Eq. (12) affects the approaching speed to the sliding surface S = 0. We increase the value of c_2^+ from 0 to 200 and 800, while retain all other control gains. The simulation responses of S for these three values of c_2^+ are shown in Fig. 6. As was expected from Eq. (12), the settling time for S decreases with the increase of c_2^+. The response for c_2^+ = 800 is almost the same as that of a first order homogenous differential equation, since the other terms on the right side of Eq. (12) are much smaller than $c_2^+ S$ in absolute value. Actually, the value of c_1^+ has similar effect on the approaching speed to the sliding surface.

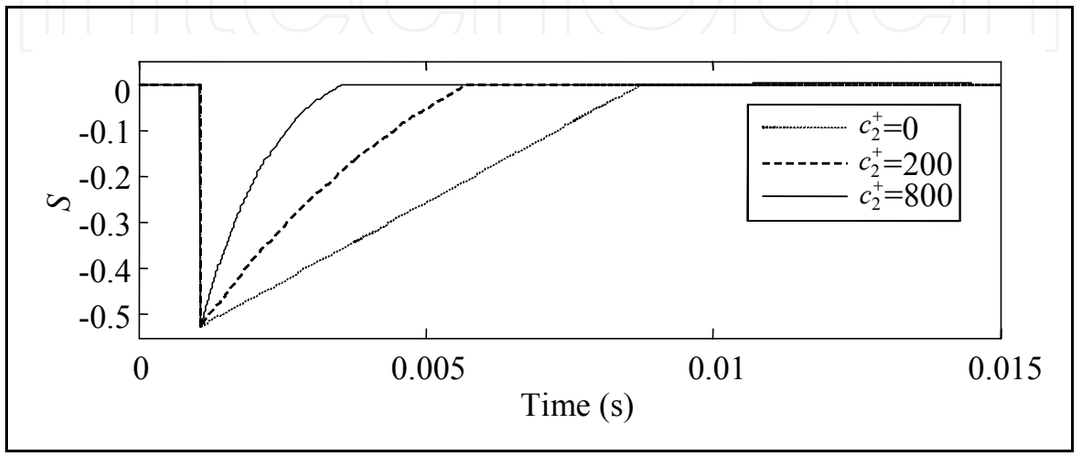

Fig. 6. Simulation responses of the sliding mode controller with various c_2^+.

We fix c_2^+ = 0 and change c_1^+ from 70 to 140 and 280. The simulation responses in Fig. 7 reveal that the settling time for S also decreases with the increase of c_1^+. However, the responses in Fig. 7 are not so smooth as those in Fig. 6. This indicates that c_2^+ is still a useful parameter to adjust the convergent speed.

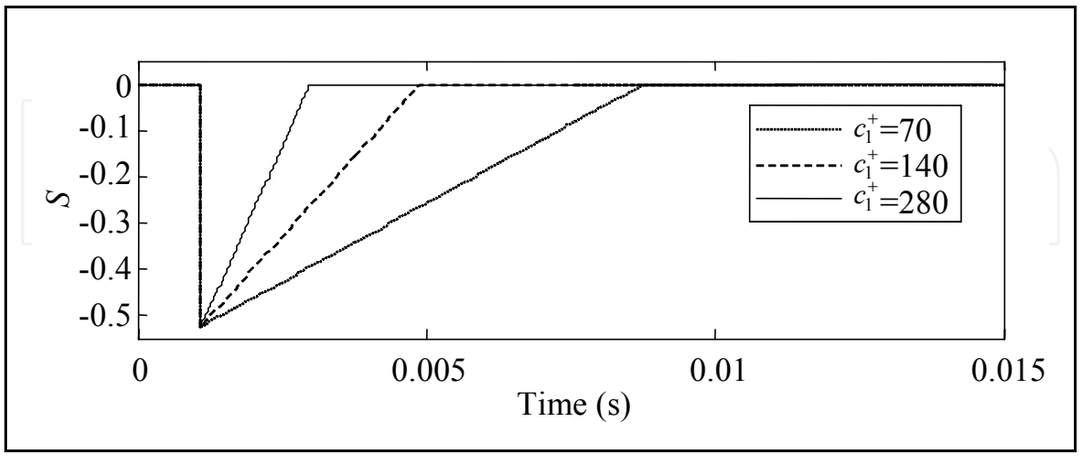

Fig. 7. Simulation responses of the sliding mode controller with various c_1^+.

Finally, we are interested in the chattering phenomenon of sliding mode control. The chattering parasitizes in the response of the sliding function S after the states reach the sliding surface S = 0. The states driven by the controller of Eq. (11) will go out of and back to

the sliding surface, since the term associated with sgn(S) changes the control effort with the direction of S. The simulation response in Fig. 8 demonstrates the existence of the chattering phenomenon in S and u for the controller with sgn(S). If we replace sgn(S) in Eq. (12) with sat(S) in Eq. (23), the chattering can be alleviated as shown by the response for the controller with sat(S) in Fig. 8.

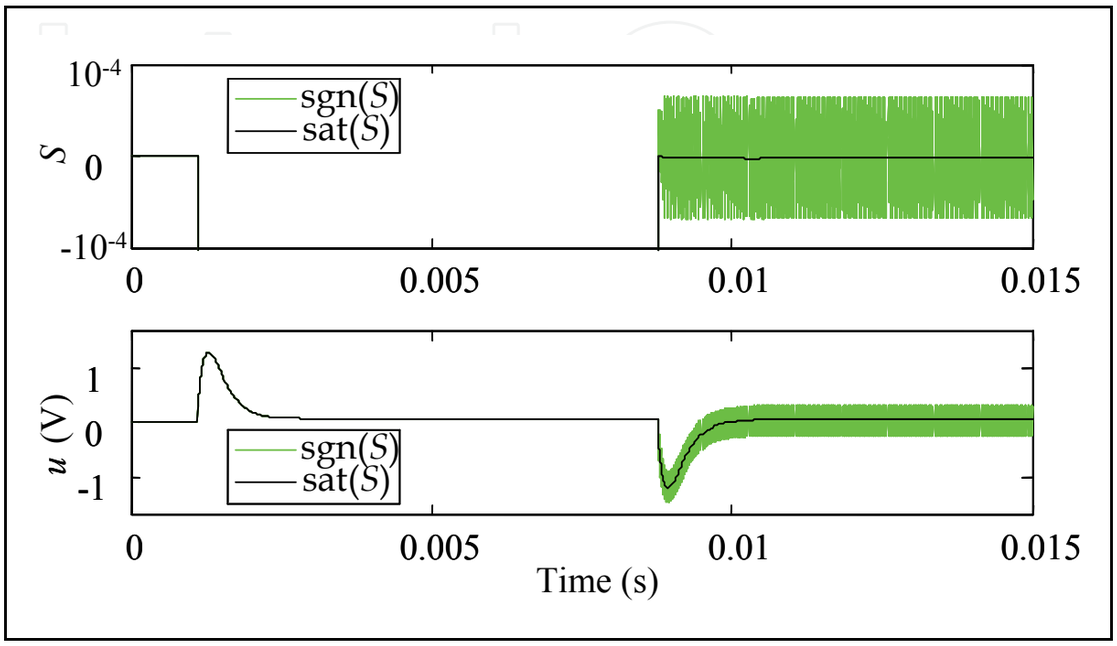

Fig. 8. Simulation responses of the sliding mode controller with sgn(S) and sat(S).

5. Experiments

The experimental setup is shown in Fig 9. The experimental system consists of a PC motherboard with X86 CPU and a FPGA board. There is a parallel ATA cable as a data communication interface. The FPGA board takes charge of generating the driving voltage of the VCM and measuring the coil current i and the actuator position d of the VCM. The PWM (Pulse Width Modulation) algorithm in the FPGA will generate the PWM signals to drive the full bridge (Chen et al., 2003) and then output the command voltage to the VCM. The full bridge plays the role of a power converter. Two ADC (analog-to-digital converter) circuits are used to sense the coil current and the actuator position, respectively. The sensed signals are filtered by the IIR filter algorithm in the FPGA. The PC motherboard reads the filtered current and position signals through the parallel ATA interface. The controller algorithm is programmed and executed in the PC motherboard. The current and position signals are the feedback signals of the controller, and are used to calculate out the controller output u. The output voltage u is then sent back, via the ATA interface, to the PWM modular of the FPGA, which transfers the voltage command to PWM signals and drives the VCM through the full bridge.

The tuning method introduced in (Ellis, 2004) is used to tune the control gains of the classic PI controller Eqs. (24)-(25). Fig. 10(a) and 10(b) shows the experimental result of the PI controller. It can be seen from Fig. 10(a) that there are stick slip oscillations after 0.15 s. The transient response in Fig. 10(b) is similar to the one of the simulation result in Fig. 5(b).

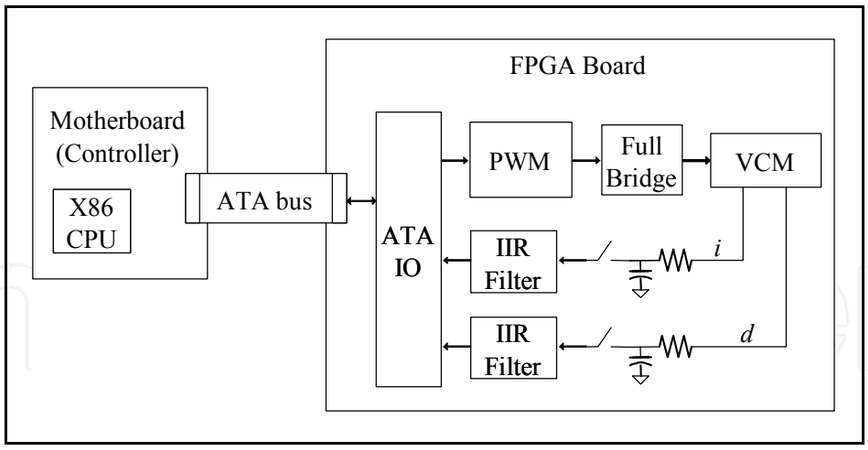

Fig. 9. Experiment system of the VCM Controller.

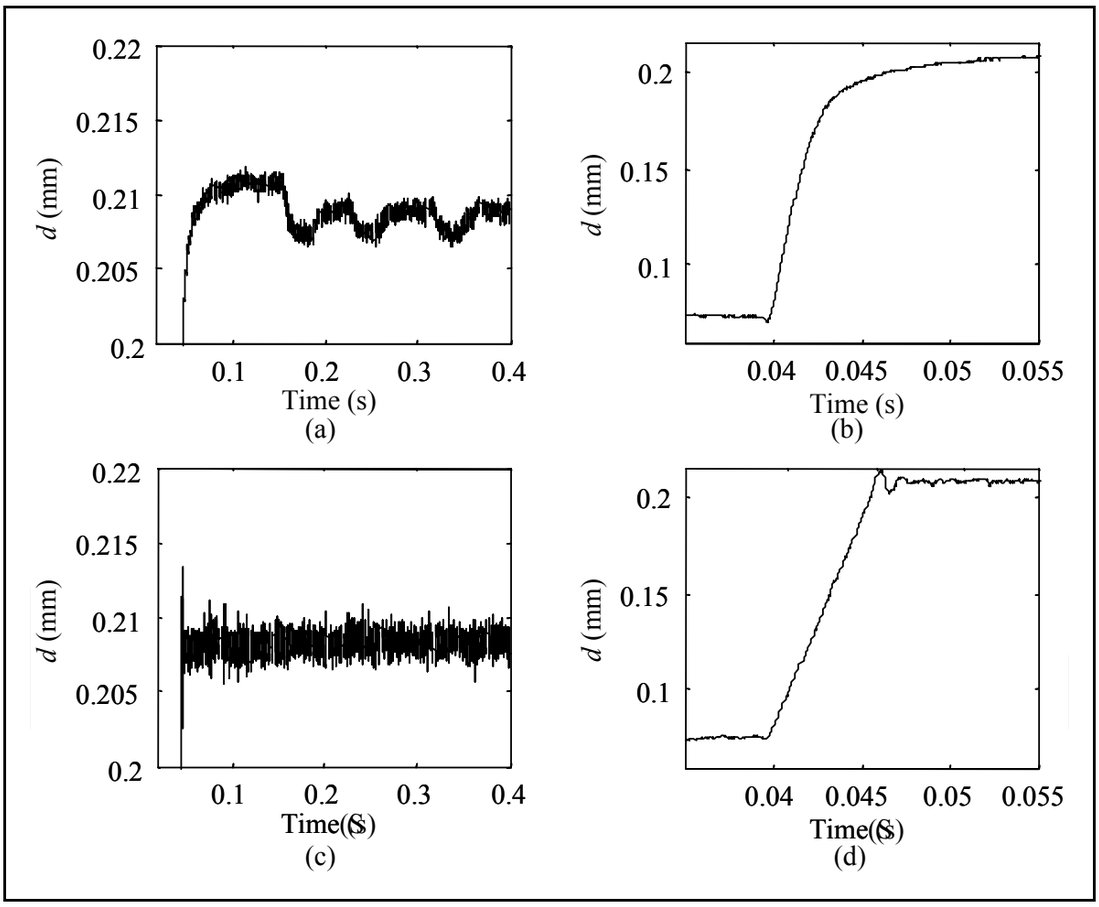

Fig. 10. Classic PI controller: (a) steady response with stick slip and (b) transient response; sliding mode controller: (c) steady response without stick slip and (d) transient response.

For the same desired position command, the experimental result of the proposed sliding mode controller has no stick slip oscillations as shown in Fig. 10(c). However, the sliding mode controller induces small overshoot in the transient response (see Fig. 10(d)), although

it has a faster response. Such a fast response is able to support the advanced AF (auto focus) algorithm capable of 60 frame-rate. It should be remarked that the response in Fig. 10(c) is noisier than that in Fig. 10(a). This is caused by the chattering of sliding mode control with sgn(S).

The difference between the responses of the sliding mode controller with sgn(S) and with sat(S) can be obtained by the experimental results shown in Fig. 11. In this experiment, the VCM is first hold in the position of d = 0.07 mm, and then is driven to the position of d = 0.22 mm. The chattering phenomenon dominates in the measured feedback coil current i in Fig. 11(b) for the controller with sgn(S). Fig. 11(d) shows that the controller with sat(S) diminishes the chattering amplitude in the coil current i. On the other hand, comparing Fig. 11(c) with Fig. 11(a) reveals that the transient response from d = 0.07 mm to d = 0.22 mm for the controller with sat(S) is smoother than that with sgn(S).

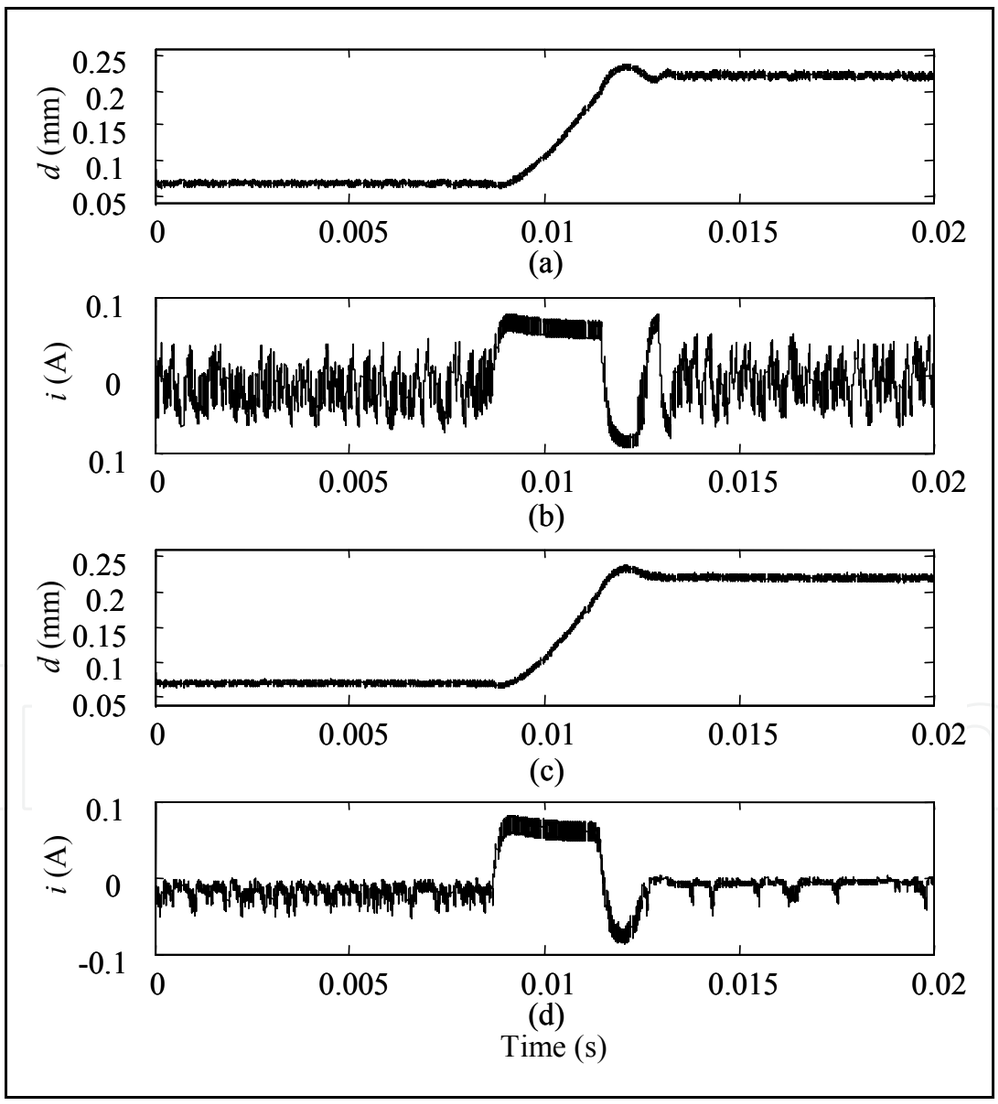

Fig. 11. Chattering phenomena: (a) and (b) responses of the controller with sgn(S); (c) and (d) responses of the controller with sat(S).

6. Repeatability tests

Repeatability is a critical specification for the VCM. In a camera, an AF (Auto Focus) algorithm detects the sharpness of images in multiple positions over the full optical stroke, and then asks the actuator to the position with the sharpest image. Poor repeatability would degrade the AF performance because the actuator would go to a wrong position different from the one with sharpest image. Thus, repeatability tests are inevitable for the VCM to be mounted in a compact camera module.

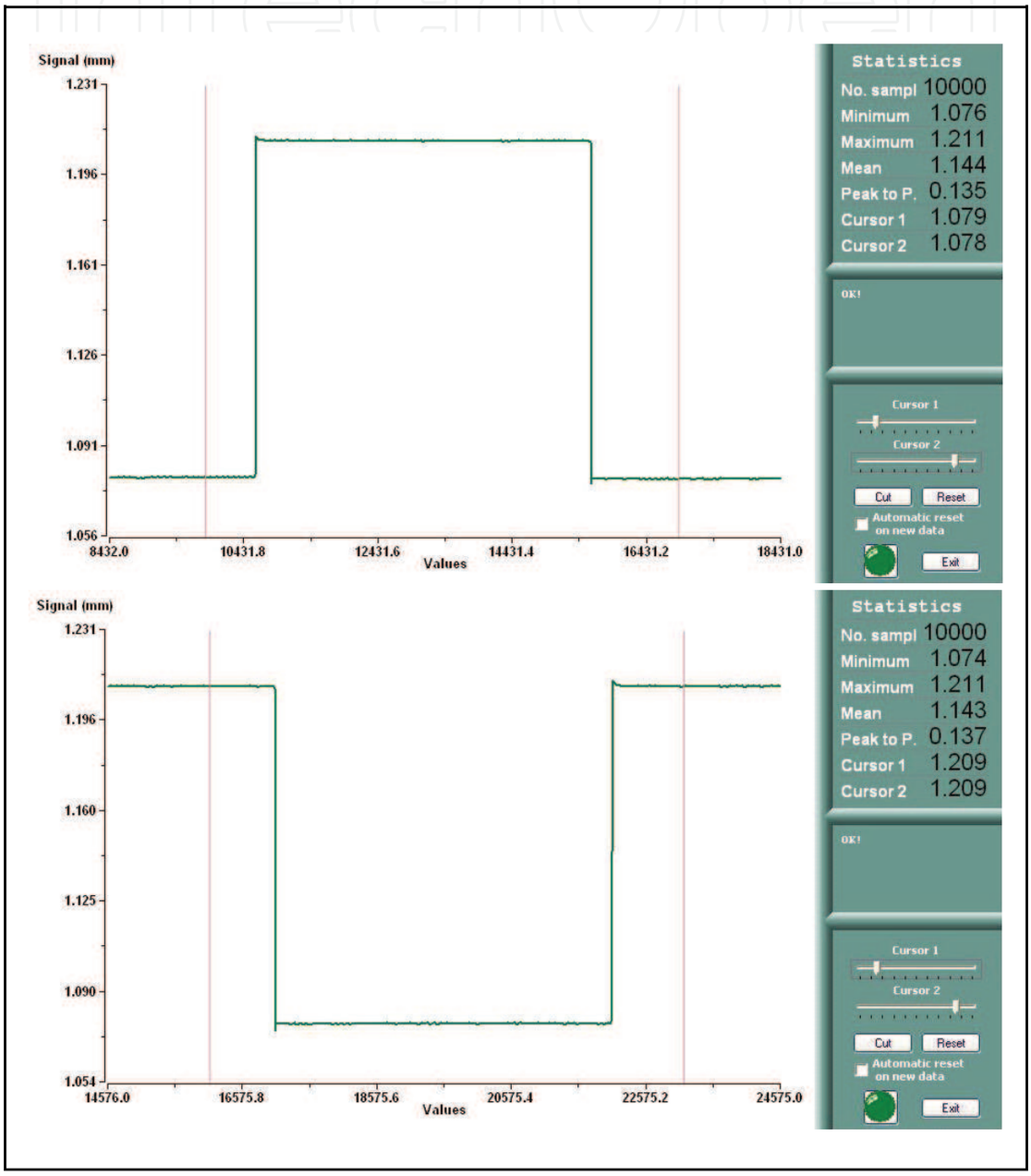

Fig. 12. LDM records for the vertical movements.

We utilize a laser displacement meter (LDM) to measure the physical position of the actuator in repeatability experiments. The controller used in the repeatability tests is only the proposed sliding mode law with sat(S). The movement of the actuator is tested both in the vertical and horizontal directions. The LDM records for the vertical movements are shown Fig. 12, while those for horizontal ones are in Fig. 13.

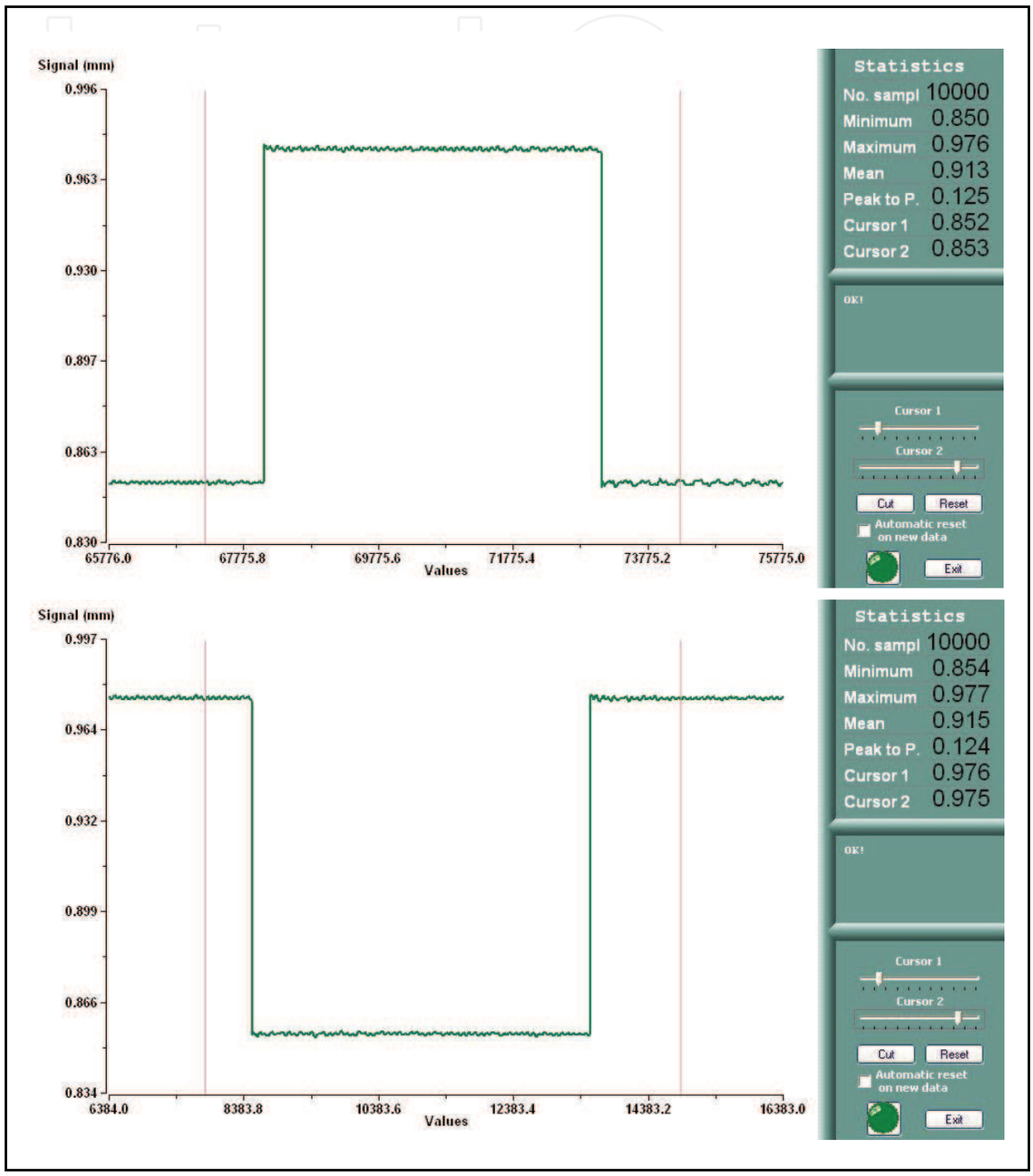

Fig. 13. LDM records for the horizontal movements.

In each record, the actuator leaves its original position and then comes back. Cursor 1 of the LDM picks the position value at an arbitrary time before leaving, while Cursor 2 picks

another one after coming back. The difference of these two values is the repeatability. The records both in Fig. 12 and in Fig. 13 have the repeatability less than or equal to 1 μm. Comparing Fig. 13 with Fig. 12, we also find that the repeatability in horizontal direction is slightly poorer. The cause is that unbalanced friction force is more largely applied on the two guide pins in this horizontal orientation. However, the nominal requirement of the repeatability for a mini camera is about 10 μm. It is of no doubt that the proposed sliding mode controller with sat(S) is suitable to drive the VCM for the AF system of a camera.

7. Conclusions

In this chapter, a sliding mode controller is proposed to compensate for the nonlinear friction force of the mini VCM mounted on a compact camera module. It is known that the stick slip friction phenomenon would result in significant image-shaking and is not allowed in the camera application. In the proposed control system, stick slip oscillations disappear and the steady state error can be designed in arbitrarily small by the pole placement in the dynamical equation of the sliding surface. The experimental results show that the transient response is less than 10 ms, no stick slip oscillations occur in the steady state response, and the repeatability performance is also excellent. Consequently, the proposed control scheme works well and is reliable.

8. Acknowledgment

This work was partially supported by the National Science Council, Taiwan under grant no. NSC 97-2221-E-009-086-MY3 and by JD Components Co., Ltd. under grant no.99C201

9. References

Bona, B. & Indri, M. (2005). Friction compensation in robotics: an overview. *Proceedings of the 44th IEEE Conference on Decision and Control and the European Control Conference 2005*, pp. 12-15, Spain, December 2005.

Canudas de Wit C.; Olsson H.; Åström K. & Lischinsky P. (1995). A new model for control of systems with friction. *IEEE Trans. on Automatic Control*, Vol. 40, No. 3, pp. 419–425.

Chen J.; Prodić A.; Erickson R. W. & Maksimović D. (2003). Predictive digital current programmed control. *IEEE Trans. on Power Electronics*, Vol. 18, No. 1, pp. 411-419.

Ellis G. H. (2004). *Control System Design Guide*, 3rd Edition, Academic Press, ISBN: 978-0-12-237461-6, San Diego.

Golnaraghi, F. & Kuo, B. C. (2009). *Automatic Control Systems*, 9th Edition, John Wiley & Sons, ISBN: 978-0470-04896-2, New York.

Hsu J. D.; Tsai C. L. & Tzou Y. Y. (2007). Design and implementation of a voice-coil motor servo control ic for auto-focus mobile camera applications. *Proceedings of 2007 IEEE 38th Annual Power Electronics Specialists Conference*, pp. 1357-1362, ISBN: 978-1-4244-0654-8, Florida, USA, June 2007.

Lin S. K.; Wang C. M. & Wang S. J. (2008). Design and implementation of anti-handshaking position control for a voice coil motor. *Journal of Applied Physics*, Vol. 103, No. 7, Art. No. 07F128, 2008.

Southward S., Radcliffe C., & MacCluer C. (1991). Robust nonlinear stick-slip friction compensation. *ASME Journal of Dynamic Systems, Measurement and Control*, Vol. 113, No. 4, pp. 639–645.

Yu H. C.; Lee T. Y.; Wang S. J.; Lai M. L.; Ju J. J.; Huang D. R. & Lin S. K. (2005). Design of a voice coil motor used in the focusing system of a digital video camera. *IEEE Transactions on Magnetics*, Vol. 41, No. 10, pp. 3979-3981.

IntechOpen

IntechOpen

Sliding Mode Control

Edited by Prof. Andrzej Bartoszewicz

ISBN 978-953-307-162-6
Hard cover, 544 pages
Publisher InTech
Published online 11, April, 2011
Published in print edition April, 2011

The main objective of this monograph is to present a broad range of well worked out, recent application studies as well as theoretical contributions in the field of sliding mode control system analysis and design. The contributions presented here include new theoretical developments as well as successful applications of variable structure controllers primarily in the field of power electronics, electric drives and motion steering systems. They enrich the current state of the art, and motivate and encourage new ideas and solutions in the sliding mode control area.

How to reference

In order to correctly reference this scholarly work, feel free to copy and paste the following:

Shir-Kuan Lin, Ti-Chung Lee and Ching-Lung Tsai (2011). Application of Sliding Mode Control to Friction Compensation of a Mini Voice Coil Motor, Sliding Mode Control, Prof. Andrzej Bartoszewicz (Ed.), ISBN: 978-953-307-162-6, InTech, Available from: http://www.intechopen.com/books/sliding-mode-control/application-of-sliding-mode-control-to-friction-compensation-of-a-mini-voice-coil-motor

INTECH
open science | open minds

InTech Europe
University Campus STeP Ri
Slavka Krautzeka 83/A
51000 Rijeka, Croatia
Phone: +385 (51) 770 447
Fax: +385 (51) 686 166
www.intechopen.com

InTech China
Unit 405, Office Block, Hotel Equatorial Shanghai
No.65, Yan An Road (West), Shanghai, 200040, China
中国上海市延安西路65号上海国际贵都大饭店办公楼405单元
Phone: +86-21-62489820
Fax: +86-21-62489821

© 2011 The Author(s). Licensee IntechOpen. This chapter is distributed under the terms of the Creative Commons Attribution-NonCommercial-ShareAlike-3.0 License, which permits use, distribution and reproduction for non-commercial purposes, provided the original is properly cited and derivative works building on this content are distributed under the same license.

IntechOpen

IntechOpen